CHALMERS

Optimization of sensor positions in magnetic tracking

Technical report

Oskar Talcoth, Thomas Rylander

Department of Signals and Systems
CHALMERS UNIVERSITY OF TECHNOLOGY
Göteborg, Sweden

R015/2011
ISSN 1403-266X

Abstract

In recent years, magnetic tracking has been applied in many biomedical settings due to the transparency of the human body to low-frequency magnetic fields. One way to improve system performance and/or reduce system cost is to optimize the sensor positions of the tracking system.

In this work, the sensor positions of a magnetic tracking system are optimized by exploiting an analytical model where the transmitting and sensing coils of the system are approximated by magnetic dipoles.

In order to compare different sensor array layouts, two performance measures based on the Fisher information matrix are discussed and compared for the optimization of the sensor positions of a circular sensor array. Furthermore, the sensor positioning problem is formulated as an optimization problem which is cast as a sensor selection problem. The sensor selection problem is solved for a planar sensor array by the application of a convex relaxation. Several transmitter positions are considered and general results are established for the dependence of the optimal sensor positions on the transmitter's position and orientation.

Contents

1 Introduction

1.1 Magnetic tracking

Magnetic tracking deals with the determination of the position and/or orientation of a specially designed marker or device by its interaction with low-frequency or static magnetic fields. This tracking technique has recently been used in numerous applications within the area of biomedical engineering. For example, Iustin et al. [1] developed a magnetic tracking system for real-time organ-positioning during radiotherapy of cancer tumors, and Plotkin et al. [2] designed a magnetic tracking system for tracking of the human eye and used it to diagnose vestibular disorders. Other biomedical applications include monitoring of heart valve prostheses [3], recognition of isolated words in silent speech by patients who have lost their larynx [4], tracking of a wireless capsule endoscope in the gastro-intestinal tract [5], catheter tracking [6, 7], and positioning of implanted medical devices embedded in a patient's bone [8]. The reason for the popularity of magnetic tracking within biomedical engineering is that the human body is transparent to low-frequency magnetic fields and, therefore, the tracking system does not have to take the details of the human body into account.

There are also non-medical applications for magnetic tracking systems, for example virtual and augmented reality [9], head tracking for helmet-mounted sights used by military pilots [10] and tracking of an American football on the football pitch [11].

1.1.1 Inverse problems

Magnetic tracking systems solve a so-called inverse problem, i.e. to find characteristic features of a source by observations or measurements of the fields caused by the source. In contrast, the forward problem deals with finding the fields from a known source. However, inverse problems are often formulated in terms of the forward problem which is solved by the forward model $\mathbf{f}^{\text{model}}(\mathbf{p})$. The forward model takes the parameters $\mathbf{p}$ that describe the source by characteristics like position and orientation as argument and returns the measured quantities, e.g. a value from a sensor that is sensitive to the field from the source.

For a non-linear model $\mathbf{f}^{\text{model}}(\mathbf{p})$, an iterative approach is normally adapted where the misfit between model and measurements $\mathbf{f}^{\text{meas}}$ is minimized by changing the parameters $\mathbf{p}$. This corresponds to solving the optimization problem

$$\underset{\mathbf{p}}{\text{minimize}} \quad J[\mathbf{f}^{\text{meas}}, \mathbf{f}^{\text{model}}(\mathbf{p})] \tag{1.1}$$

where J is a suitable cost function(-al) that measures the difference between its

arguments. The most commonly chosen cost function is

$$J[\mathbf{f}^{\text{meas}}, \mathbf{f}^{\text{model}}(\mathbf{p})] = ||\mathbf{f}^{\text{meas}} - \mathbf{f}^{\text{model}}(\mathbf{p})||^2_{L^2}. \tag{1.2}$$

The solution to the optimization problem, i.e. the set of parameters that minimizes the misfit between model and measurements, constitutes the solution to the inverse problem. For magnetic tracking systems, certain system designs allow for an estimation process where $\mathbf{p}$ can be determined directly and, consequently, an iterative procedure can be avoided.

1.2 System designs

Magnetic tracking systems exploit either static magnetic fields, as in for example reference [4], or low-frequency alternating magnetic fields, as in for example reference [2]. In the static case, permanent magnets are normally used as sources and the field is measured by Hall sensors. The corresponding function is usually fulfilled by coils in the case with alternating fields, where the source often is referred to as a transmitter and the sensor as a receiver. The tracked object is often equipped with a receiver that is exposed to the field due to a set of transmitters. However, several systems are operated in the reversed manner and, consequently, the position and orientation of one transmitter is determined by measuring the field with several receivers. In the following, we refer to such a system if not stated otherwise.

To allow for identification of the individual transmitted signals in a multi-transmitter system, multiplexing in time or frequency is normally used. This is not needed in a uni-transmitter system. The most common multi-transmitter arrangement is a flat array, cf. reference [12]. However, several other arrangements exist, for example multiple multi-axial transmitters as described in reference [13]. Naturally, the receivers can also be uni-axial, bi-axial and tri-axial. Further system designs are discussed by Plotkin et al. [14]. In addition, there are examples of receivers that measure both the magnetic field and its gradient as described in reference [15]. Iustin et al. [1] presented a system with passive magnetic shielding that mitigates problems associated with unknown objects in the vicinity of the measurement region. Consequently, the design process of a magnetic tracking system involves several decisions and such design considerations are presented by Shafrir et al. [16].

1.3 Optimal measurements

In general, more sensors give higher accuracy in the estimated parameters, see for example reference [17] for such a result for magnetic tracking systems. However, the system cost, complexity, size etc. limit the number of sensors that can be used. Furthermore, measurement and processing time generally increases as the number of sensors is increased, which may be a restriction for real-time systems used for control purposes. Therefore, it is of great interest to maximize the information collected by

the available sensors. One possible way of achieving this is to optimize the sensor positions. Ucinski summarizes this on page 2 of reference [18]:

> "*The location of sensors is not necessarily dictated by physical considerations or by intuition and, therefore, some systematic approaches should still be developed in order to reduce the cost of instrumentation and to increase the efficiency of identifiers.*"

The optimization of sensor positions is a central part of the field of optimal measurements, a field that is also known as design of experiments. The field has many applications in spatial statistics, where problems from geology, agriculture, meteorology etc. are treated. Introductions to the field have been written by Ucinski [18], Pukelsheim [19], Atkinson et al. [20], and Walter et al. [21]. A short introduction is also given in section 3 of this report.

The theory of optimal measurements has been applied to hydrophone-based source localization [22], robotics [23] and target tracking with moving targets [24], among other applications. As to electromagnetic applications of optimal measurements, Nordebo et al. [25] optimized a measurement set-up for the estimation of antenna near-fields.

1.4 Scope of this work

Our overall aim is to optimize the sensor positions of the magnetic tracking system described in reference [1]. In this work, we aim to formulate a performance measure that can be used for comparison between different sensor array layouts and to use this measure for the optimization of sensor arrays with different topology. To achieve this, we model a generic magnetic tracking system in section 2. Performance measures are proposed and an optimization problem is formulated in section 3 whereas section 4 presents results from the optimization of planar sensor arrays.

2 Modeling

2.1 Introduction

Modeling of a magnetic tracking system is always needed since the model is used in the parameter estimation process. Static and low-frequency alternating magnetic fields are usually modeled using the same models by the use of quasi-static approximations for the alternating fields. A commonly used model, see for example references [3, 10, 12], is the one which models both transmitting and receiving coils as magnetic dipoles. Such a model is valid when the distance between the transmitting and the receiving coil is large compared to the coils' dimensions. In contrast, Plotkin et al. [2] used a more elaborate model based on the Biot-Savart law, which is accurate even at small distances. Under the assumption that the model based on the Biot-Savart law is correct, the relative error of the dipole model was investigated by Roetenberg et al. [26] for circular coils and by Baszynski et al. [27] for square coils. On an axis perpendicular to the sensor plane and passing through the coil's midpoint, both studies reported an relative error of 1 % at a distance of 6 coil diameters and 6 coil side lengths respectively.

An alternative approach was taken by Ge et al. [28]. For a tri-axial receiver at a certain distance from a transmitter, the amplitude of the received signal is maximized by pointing the magnetic moment of the transmitter straight at the receiver. If several transmitters are pointing at the receiver, the receiver position can easily be obtained by triangulation. Ge et al. [28] proposed to exploit this with a system that included several transmitters which could point in an arbitrary direction. The main difficulty of such an approach is how to make the transmitters point straight at the receiver. Unfortunately, this was not commented on, nor explained by the authors. In particular, the received signal is insensitive to small deviations of the transmitter orientation from the correct orientation.

Modeling errors, interference from magnetic and/or metal objects in the surroundings, mutual coupling between coils, an ill-designed parameter estimation procedure, and other factors can degrade the positioning performance. Several methods have been proposed to mitigate these effects. For example, compensation for fixed objects in the surrounding was proposed by Raab et al. [10] and calibration procedures were used by Plotkin et al. [29] and Li et al. [30], whereas Plotkin et al. [2] measured the crosstalk present in the system and compensated for it in the model.

Instead of modeling the true system as accurately as possible, Paperno et al. [31] searched for coil designs which yield a magnetic field in the vicinity of the coil that resembles the ideal magnetic dipole field as closely as possible.

Iustin et al. [1] went one step further and generated surrogate models from measurement data obtained with the transmitter in known positions. Compensation for all

types of imperfections is thus possible at the expense of a lengthy calibration procedure needed to construct the surrogate model. The performance of this method is highly dependent on the ability of the surrogate model to model the true system. In addition, changes in the system and its surroundings between calibration and positioning can degrade the performance of the system.

2.2 Dipole-based model

We model a generic single-frequency magnetic tracking system. The transmitting and receiving coils are approximated by magnetic dipoles in free space. This approximation is valid when the distance between transmitter and receiver is large compared to the size of the coil. Furthermore, the model can include an infinite plane of a perfect magnetic conductor (PMC).

Magnetic tracking systems generally operate at frequencies lower than 200 kHz. At 200 kHz, the wavelength is approximately 1.5 km and the phase variation of the magnetic field over the size of a magnetic tracking system is very small. Thus, we exploit a quasi-static approximation and only consider the amplitude of the magnetic field. The fields below are expressed as phasors such that $f(t) = \mathrm{Re}\{f(\omega)\exp(j\omega t)\}$ where j is the imaginary unit, ω the angular frequency, and t the time.

The magnetic vector potential, $\vec{A}$, for a magnetic dipole is [32]

$$\vec{A}(\vec{R}) = \mu_0 \frac{\vec{m}^{\mathrm{trans}} \times \vec{R}}{4\pi R^3} \tag{2.1}$$

where μ_0 is the permeability of free space, $\vec{m}^{\mathrm{trans}}$ is the magnetic moment of the dipole, and $\vec{R} = \vec{r} - \vec{r}^{\,\mathrm{trans}}$ is the vector of length R from the position of the dipole $\vec{r}^{\,\mathrm{trans}}$ to the evaluation point $\vec{r}$. The corresponding magnetic flux density $\vec{B}$ is obtained from

$$\vec{B} = \nabla \times \vec{A}(\vec{R}) \tag{2.2}$$

as

$$\vec{B} = \frac{\mu_0}{4\pi}\left(\frac{3(\vec{m}^{\mathrm{trans}} \cdot \vec{R})\vec{R}}{R^5} - \frac{\vec{m}^{\mathrm{trans}}}{R^3}\right). \tag{2.3}$$

If a receiver coil with number k is placed in this magnetic field at $\vec{r}_k^{\,\mathrm{rec}}$, a voltage V is induced in the coil and it can be expressed according to Faraday's law as

$$\begin{aligned} V = &- j\omega\alpha^{\mathrm{rec}}\hat{m}^{\mathrm{rec}} \cdot \vec{B} = \\ &- j\omega\alpha^{\mathrm{rec}}\alpha^{\mathrm{trans}} I^{\mathrm{trans}} \frac{\mu_0}{4\pi}\left(\frac{3(\hat{m}^{\mathrm{trans}} \cdot \vec{R})(\hat{m}^{\mathrm{rec}} \cdot \vec{R})}{R^5} - \frac{\hat{m}^{\mathrm{trans}} \cdot \hat{m}^{\mathrm{rec}}}{R^3}\right) \end{aligned} \tag{2.4}$$

where α^{rec} is the number of turns times the area of the receiving coil, α^{trans} the corresponding quantity for the transmitting coil, I^{trans} is the amplitude of the current

in the transmitting coil, $\vec{R} = \vec{r}_k^{\,\mathrm{rec}} - \vec{r}^{\,\mathrm{trans}}$, and unit vectors are indicated by a hat. The introduction of a constant

$$\alpha = j\omega\alpha^{\mathrm{rec}}\alpha^{\mathrm{trans}}I^{\mathrm{trans}} \tag{2.5}$$

simplifies the notation of the induced voltage to

$$V = -\alpha\frac{\mu_0}{4\pi}\left(\frac{3(\hat{m}^{\mathrm{trans}}\cdot\vec{R})(\hat{m}^{\mathrm{rec}}\cdot\vec{R})}{R^5} - \frac{\hat{m}^{\mathrm{trans}}\cdot\hat{m}^{\mathrm{rec}}}{R^3}\right). \tag{2.6}$$

As can be seen in equation (2.6), the expression is symmetric in $\hat{m}^{\mathrm{trans}}$ and $\hat{m}^{\mathrm{rec}}$ which makes the model invariant to changes in which coil acts as transmitter and which coil acts as receiver (the only modification needed is in equation (2.5) where I^{trans} should be changed to I^{rec}). This is a consequence of the reciprocity of the mutual inductance between two circuits in linear media.

2.2.1 Linearization and derivatives

In order to optimize the sensor positions (see section 3 below) the model described above will be linearized. We therefore need to find the partial derivatives of the induced voltage with respect to the position and direction of the transmitter. Receiver electronics in the system can also be included in these derivatives and linearized, should non-linearities be present.

The gradient of the voltage with respect to the position of the transmitter is given by

$$\begin{aligned}\nabla_{(\vec{r}^{\,\mathrm{trans}})}V &= \left[\frac{\partial V}{\partial x^{\mathrm{trans}}}, \frac{\partial V}{\partial y^{\mathrm{trans}}}, \frac{\partial V}{\partial z^{\mathrm{trans}}}\right]^T = \\ &= -\alpha\frac{\mu_0}{4\pi}\left(15\frac{(\hat{m}^{\mathrm{trans}}\cdot\vec{R})(\hat{m}^{\mathrm{rec}}\cdot\vec{R})\vec{R}}{R^7}\right. \\ &\qquad \left. - 3\frac{(\hat{m}^{\mathrm{trans}}\cdot\vec{R})\hat{m}^{\mathrm{rec}} + (\hat{m}^{\mathrm{rec}}\cdot\vec{R})\hat{m}^{\mathrm{trans}} + (\hat{m}^{\mathrm{trans}}\cdot\hat{m}^{\mathrm{rec}})\vec{R}}{R^5}\right).\end{aligned} \tag{2.7}$$

The gradient of the voltage with respect to the position of the sensor is

$$\nabla_{(\vec{r}^{\,\mathrm{rec}})}V = -\nabla_{(\vec{r}^{\,\mathrm{trans}})}V, \tag{2.8}$$

and the gradient of the voltage with respect to the magnetic moment of the transmitter is given by

$$\nabla_{(\vec{m}^{\mathrm{trans}})}V = \left[\frac{\partial V}{\partial \vec{m}_x^{\mathrm{trans}}}, \frac{\partial V}{\partial \vec{m}_y^{\mathrm{trans}}}, \frac{\partial V}{\partial \vec{m}_z^{\mathrm{trans}}}\right]^T = -\alpha\frac{\mu_0}{4\pi}\left(\frac{3(\hat{m}^{\mathrm{rec}}\cdot\vec{R})\vec{R}}{R^5} - \frac{\hat{m}^{\mathrm{rec}}}{R^3}\right). \tag{2.9}$$

If we introduce a spherical coordinate system defined by

$$\begin{cases} x = \rho \sin\theta \cos\varphi \\ y = \rho \sin\theta \sin\varphi \\ z = \rho \cos\theta \end{cases} \tag{2.10}$$

with its origin at the transmitting dipole, we can find the derivative of the induced voltage with respect to the magnetic moment expressed in these coordinates. This is useful when the dipole is rotated without changing the value of its magnetic moment. Application of the chain rule gives

$$\begin{aligned} \begin{bmatrix} \frac{\partial V}{\partial \vec{m}_\rho^{\text{trans}}} \\ \frac{\partial V}{\partial \vec{m}_\theta^{\text{trans}}} \\ \frac{\partial V}{\partial \vec{m}_\varphi^{\text{trans}}} \end{bmatrix} &= \begin{bmatrix} \frac{\partial x}{\partial \rho} & \frac{\partial y}{\partial \rho} & \frac{\partial z}{\partial \rho} \\ \frac{\partial x}{\partial \theta} & \frac{\partial y}{\partial \theta} & \frac{\partial z}{\partial \theta} \\ \frac{\partial x}{\partial \varphi} & \frac{\partial y}{\partial \varphi} & \frac{\partial z}{\partial \varphi} \end{bmatrix} \begin{bmatrix} \frac{\partial V}{\partial \vec{m}_x^{\text{trans}}} \\ \frac{\partial V}{\partial \vec{m}_y^{\text{trans}}} \\ \frac{\partial V}{\partial \vec{m}_z^{\text{trans}}} \end{bmatrix} = \\ &= \begin{bmatrix} \sin\theta\cos\varphi & \sin\theta\sin\varphi & \cos\theta \\ \rho\cos\theta\cos\varphi & \rho\cos\theta\sin\varphi & -\rho\cos\theta \\ -\rho\sin\theta\sin\varphi & \rho\sin\theta\cos\varphi & 0 \end{bmatrix} \begin{bmatrix} \frac{\partial V}{\partial \vec{m}_x^{\text{trans}}} \\ \frac{\partial V}{\partial \vec{m}_y^{\text{trans}}} \\ \frac{\partial V}{\partial \vec{m}_z^{\text{trans}}} \end{bmatrix}. \end{aligned} \tag{2.11}$$

2.2.2 Infinite perfect magnetic conductor plane

Different types of magnetic materials can be used in situations where the magnetic tracking system needs to be shielded or have its signal strength improved. We model one such situation by the possibility to include an infinite plane modeled as a PMC with normal vector $\hat{n}$. Consider a PMC plane defined by $z = 0$ and a source located in the half space $z > 0$. The corresponding fields and gradients in the region $z > 0$ can easily be computed by the method of images. The PMC plane is replaced by artificial image sources in the region $z < 0$ such that the boundary condition for the magnetic field $\vec{H}$ is satisfied on the PMC, i.e.

$$\hat{n} \times \vec{H} = \vec{0}. \tag{2.12}$$

A magnetic dipole situated at $\vec{r} = (x, y, z), z > 0$ with magnetic moment $\vec{m} = (m_x, m_y, m_z)$ is imaged with a dipole at $\vec{r}^{\,\text{image}} = \vec{r} - 2(\hat{n} \cdot \vec{r})\hat{n} = (x, y, -z)$ and magnetic moment $\vec{m}^{\,\text{image}} = 2(\hat{n} \cdot \vec{m})\hat{n} - \vec{m} = (-m_x, -m_y, m_z)$ in order to fulfill the boundary condition on the PMC.

The total derivative (denoted with the superscript tot) of the induced voltage in a receiving coil placed in the half space $z > 0$ is given as a function of the derivative

of the original dipole (superscript ori) and the image dipole (superscript img) as

$$\begin{aligned}
\frac{\partial V^{\mathrm{tot}}}{\partial x^{\mathrm{i}}} &= \frac{\partial V^{\mathrm{ori}}}{\partial x^{\mathrm{i}}} + \frac{\partial V^{\mathrm{img}}}{\partial x^{\mathrm{i}}} \\
\frac{\partial V^{\mathrm{tot}}}{\partial y^{\mathrm{i}}} &= \frac{\partial V^{\mathrm{ori}}}{\partial y^{\mathrm{i}}} + \frac{\partial V^{\mathrm{img}}}{\partial y^{\mathrm{i}}} \\
\frac{\partial V^{\mathrm{tot}}}{\partial z^{\mathrm{i}}} &= \frac{\partial V^{\mathrm{ori}}}{\partial z^{\mathrm{i}}} - \frac{\partial V^{\mathrm{img}}}{\partial z^{\mathrm{i}}} \\
\frac{\partial V^{\mathrm{tot}}}{\partial \vec{m}_x^{\mathrm{i}}} &= \frac{\partial V^{\mathrm{ori}}}{\partial \vec{m}_x^{\mathrm{i}}} - \frac{\partial V^{\mathrm{img}}}{\partial \vec{m}_x^{\mathrm{i}}} \\
\frac{\partial V^{\mathrm{tot}}}{\partial \vec{m}_y^{\mathrm{i}}} &= \frac{\partial V^{\mathrm{ori}}}{\partial \vec{m}_y^{\mathrm{i}}} - \frac{\partial V^{\mathrm{img}}}{\partial \vec{m}_y^{\mathrm{i}}} \\
\frac{\partial V^{\mathrm{tot}}}{\partial \vec{m}_z^{\mathrm{i}}} &= \frac{\partial V^{\mathrm{ori}}}{\partial \vec{m}_z^{\mathrm{i}}} + \frac{\partial V^{\mathrm{img}}}{\partial \vec{m}_z^{\mathrm{i}}}
\end{aligned} \tag{2.13}$$

where $\mathrm{i} \in \{\mathrm{trans}, \mathrm{rec}\}$. The derivatives with respect to the magnetic moment expressed in spherical coordinates are given by application of the transformation in equation (2.11) on the total derivatives from equation (2.13).

An infinite non-magnetic half-space $z < 0$ of finite conductivity can be approximated by complex image theory as presented in reference [33], where the source is imaged in a plane that coincides with $z = z^{\mathrm{image}} < 0$ with z^{image} as a function of the skin depth. Arumugam et al. [11] used this theory for a magnetic tracking system.

3 Optimization of sensor positions

3.1 Introduction

Gilbert et al. [4] took an engineering approach to the optimization of sensor positions for tracking of body parts involved in speech production. Modeling was combined with clinical considerations to "*maximise sensitivity to desired articulator movement while minimising the effect of implant/sensor misplacement and misorientation*". In contrast, Shafrir et al. [16] adopted a more structured approach and employed a two-step evolutionary algorithm to optimize the sensor positions of a magnetic tracking system in the minimax sense, i.e. the worst-case performance was maximized. The optimization suffered from long simulation times, partly due to the fact that "[they] *had to run* 10^3 *iterations of the tracking algorithm*" for each transmitter position in order to evaluate the tracking error caused by additive white noise in the measured signals. Thus, there is a need for more sophisticated performance measures to be incorporated in structured optimization methods for the problem at hand.

In order to find such performance measures, we use concepts and theory from the field of design of experiments and optimal measurements. The literature is vast and we refer to the textbooks [18, 19, 20, 21] for an introduction. Applications of optimal measurements in an electromagnetic context are rare and one example is the work by Nordebo et al. [25] who used multi-pole expansions and theory on optimal measurements to optimize a measurement set-up for antenna near-field estimation.

3.2 Performance measure

In order to optimize the sensor positions, a performance measure is needed that permits different sensor array layouts to be compared to each other. In the optimization procedure, a sensor array layout is sought that maximizes the performance measure.

We express our performance measure in terms of the so-called Fisher information matrix (FIM) which is derived in section 3.2.1. One such performance measure is based on the concept of D-optimality which is introduced in section 3.2.2.

3.2.1 Fisher information

Consider a situation where we want to determine the five degrees of freedom of a transmitting magnetic dipole (we assume that the total magnetic moment is known) by measuring the induced voltage in each of the sensors in a sensor array. Let $\mathbf{p} \in \mathbb{R}^p$

denote the vector of parameters that we want to estimate. In our case, the parameter vector includes the three spatial coordinates of the transmitter as well as the two angles that describe its orientation, i.e. $p = 5$ and

$$\mathbf{p} = \left[x^{\text{trans}}, y^{\text{trans}}, z^{\text{trans}}, \theta^{\text{trans}}, \varphi^{\text{trans}}\right]^T \tag{3.1}$$

where $\mathbf{a}^T$ denotes the transpose of a vector $\mathbf{a}$. Assume that the position and direction of the transmitting dipole is described by $\mathbf{p}_0$, that is a point in the parameter space. The signal measured by the N^{rec} sensors $\mathbf{V}^{\text{meas}}(\mathbf{p}_0) \in \mathbb{R}^{N^{\text{rec}}}$ is modeled as the true signal $\mathbf{V}(\mathbf{p}_0)$ plus additive Gaussian noise as

$$\begin{aligned} \mathbf{V}^{\text{meas}}(\mathbf{p}_0) &= \mathbf{V}(\mathbf{p}_0) + \mathbf{n}, \\ \mathbf{n} &\in \mathcal{N}(\mathbf{0}, \sigma^2\mathbf{I}) \end{aligned} \tag{3.2}$$

where the entries of $\mathbf{n} \in \mathbb{R}^{N^{\text{rec}}}$ are independent and identically distributed (i.i.d), $\mathcal{N}(\mu, \mathbf{C})$ denotes the multivariate Gaussian distribution with mean $\mu \in \mathbb{R}^{N^{\text{rec}}}$ and covariance matrix $\mathbf{C} \in \mathbb{R}^{N^{\text{rec}} \times N^{\text{rec}}}$, and $\mathbf{I}$ is the N^{rec}-dimensional identity matrix. Now, express the true signal as a Taylor expansion in the parameter space around the point $\mathbf{p}_0$ as

$$\mathbf{V}(\mathbf{p}_0 + \delta\mathbf{p}) = \mathbf{V}(\mathbf{p}_0) + \nabla_{\mathbf{p}}\mathbf{V}(\mathbf{p}_0)\delta\mathbf{p} + \text{H.O.T.} \tag{3.3}$$

where $\delta\mathbf{p}$ is the deviation from $\mathbf{p}_0$, H.O.T signifies higher order terms, and

$$\nabla_{\mathbf{p}}\mathbf{V}(\mathbf{p}_0) = \mathbf{G} = \begin{bmatrix} \nabla_{\mathbf{p}} V_1(\mathbf{p}_0)^T \\ \nabla_{\mathbf{p}} V_2(\mathbf{p}_0)^T \\ \vdots \\ \nabla_{\mathbf{p}} V_{N^{\text{rec}}}(\mathbf{p}_0)^T \end{bmatrix} \tag{3.4}$$

is the sensitivity matrix where V_i is the signal measured with receiver i. By neglecting the higher order terms in equation (3.3) and equating this expression with the expression for the measured signal in equation (3.2) we obtain

$$\mathbf{G}\delta\mathbf{p} = -\mathbf{n} \tag{3.5}$$

and

$$\delta\mathbf{p} = -\mathbf{G}^{-1}\mathbf{n} \tag{3.6}$$

where $\mathbf{G}^{-1}$ denotes the (pseudo-)inverse.

Following from the behavior of the multivariate normal distribution under affine transformations[1] and equations (3.2) and (3.6), we get

$$\delta\mathbf{p} \in \mathcal{N}(\mathbf{0}, \mathbf{G}^{-1}\sigma^2\mathbf{I}(\mathbf{G}^{-1})^T) = \mathcal{N}(\mathbf{0}, \sigma^2(\mathbf{G}^T\mathbf{G})^{-1}). \tag{3.7}$$

[1] If $\mathbf{X} \in \mathcal{N}(\mu, \mathbf{\Sigma})$ then $\mathbf{Y} = \mathbf{c} + \mathbf{B}\mathbf{X} \in \mathcal{N}(\mathbf{c} + \mathbf{B}\mu, \mathbf{B}\mathbf{\Sigma}\mathbf{B}^T)$ where $\mathbf{X}, \mu \in \mathbb{R}^m$, $\mathbf{\Sigma} \in \mathbb{R}^{m \times m}$, $\mathbf{Y}, \mathbf{c} \in \mathbb{R}^n$, and $\mathbf{B} \in \mathbb{R}^{n \times m}$.

The Fisher information matrix $\mathbf{M} = \mathbf{G}^T\mathbf{G} \in \mathbb{R}^{p\times p}$ corresponds to a sum of the sensors' individual Fisher information matrices as

$$\begin{aligned}\mathbf{M} = \mathbf{G}^T\mathbf{G} &= \sum_{i=1}^{N^{\text{rec}}} \mathbf{M}_i = \\ &= \sum_{i=1}^{N^{\text{rec}}} \begin{bmatrix} \left(\frac{\partial V_i}{\partial x^{\text{trans}}}\right)^2 & \left(\frac{\partial V_i}{\partial x^{\text{trans}}}\right)\left(\frac{\partial V_i}{\partial y^{\text{trans}}}\right) & \cdots & \left(\frac{\partial V_i}{\partial x^{\text{trans}}}\right)\left(\frac{\partial V_i}{\partial \varphi^{\text{trans}}}\right) \\ \vdots & & & \vdots \\ \left(\frac{\partial V_i}{\partial \varphi^{\text{trans}}}\right)\left(\frac{\partial V_i}{\partial x^{\text{trans}}}\right) & \left(\frac{\partial V_i}{\partial \varphi^{\text{trans}}}\right)\left(\frac{\partial V_i}{\partial y^{\text{trans}}}\right) & \cdots & \left(\frac{\partial V_i}{\partial \varphi^{\text{trans}}}\right)^2 \end{bmatrix}.\end{aligned} \tag{3.8}$$

Note that this relationship holds true only when the noise terms are independent. From equation (3.7), we see that the deviation of our estimate from the true value depends on the inverse of the FIM. Maximizing, in some sense, the FIM therefore corresponds to minimizing the errors in the estimated parameters that are due to the noise. This follows from the Cramér-Rao inequality, see [21],

$$\operatorname{cov}\hat{\mathbf{p}} \succeq \mathbf{M}^{-1} \tag{3.9}$$

which gives a lower bound for the covariance of the estimated parameter $\hat{\mathbf{p}}$ for an unbiased estimator. Note that the inequality should be understood in the sense that $\mathbf{A} \succeq \mathbf{B}$ is equivalent to $\mathbf{A} - \mathbf{B} \succeq \mathbf{0}$ which corresponds to that $\mathbf{A} - \mathbf{B}$ is positive semi-definite.

The FIM can be derived and interpreted in several other ways. For example, the FIM can be seen as the Hessian of the least-squares criterion, i.e. the l^2-norm of the difference between the measured values and their modeled counterparts [18]. Furthermore, the FIM is also closely related to the Hessian of the log-likelihood with respect to the estimated parameters [21].

3.2.2 D-optimality

It is, in general, not possible [18] to find an optimal FIM, i.e. a $\mathbf{M}^*(\mathbf{p})$ such that

$$\mathbf{M}^*(\mathbf{p}) \succeq \mathbf{M}(\mathbf{p}),\ \forall \mathbf{M} \neq \mathbf{M}^*. \tag{3.10}$$

Therefore, one often seeks to minimize some real-valued function $\Psi(\mathbf{M})$. There exists a vast number of such functions, see for example references [18] and [20], from which we have chosen the standard choice

$$\Psi(\mathbf{M}) = -\ln\det(\mathbf{M}). \tag{3.11}$$

Successful minimization of this function leads to a so-called D-optimal solution where the D stands for determinant. (Many of the alternatives to this function are described with other letters such as A, E, and T wherefore the derogatory term *alphabetic criteria* sometimes is used). The D-criterion is intended to minimize the volume of the uncertainty ellipsoid (for a fixed noise level) described by $\mathbf{M}^{-1}$ in equation (3.9). One attractive feature of the D-criterion is that it is invariant to the scaling of the estimated parameters [18].

3.2.3 D_s-optimality

In some situations, only a subset of the parameters in $\mathbf{p}$ are of interest but the entire set of parameters needs to be estimated in order to achieve a successful estimation. For example, in magnetic tracking only the position of the transmitter might be of interest, but the estimation algorithm is formulated such that also the orientation of the transmitter must be estimated concurrently. Parameters that are of no interest except that they are needed in the estimation process are called *nuisance parameters*.

In contrast to D-optimality where the determinant of the entire inverse of $\mathbf{M}$ is minimized, D_s-optimality is intended to minimize the determinant of the block of $\mathbf{M}^{-1}$ that is related to the interesting parameters.

Assume that we are interested in the first p_s parameters of $\mathbf{p}$. The D_s-optimality criterion is then the determinant of the $p_s \times p_s$ upper left block of $\mathbf{M}^{-1}$. The complete inversion of $\mathbf{M}$ can be avoided by using the following formulas from reference [21]. Let

$$\mathbf{M} = \begin{bmatrix} \mathbf{M}_{11} & \mathbf{M}_{12} \\ \mathbf{M}_{21} & \mathbf{M}_{22} \end{bmatrix}, \tag{3.12}$$

assume that $\mathbf{M}_{22}$ is non-singular and let

$$\mathbf{\Gamma} = \mathbf{M}_{11} - \mathbf{M}_{12}\mathbf{M}_{22}^{-1}\mathbf{M}_{21}.$$

The inverse of $\mathbf{M}$ is then given by

$$\mathbf{M}^{-1} = \begin{bmatrix} \mathbf{\Gamma}^{-1} & -\mathbf{\Gamma}^{-1}\mathbf{M}_{12}\mathbf{M}_{22}^{-1} \\ -\mathbf{M}_{22}^{-1}\mathbf{M}_{21}\mathbf{\Gamma}^{-1} & \mathbf{M}_{22}^{-1} + \mathbf{M}_{22}^{-1}\mathbf{M}_{21}\mathbf{\Gamma}^{-1}\mathbf{M}_{12}\mathbf{M}_{22}^{-1} \end{bmatrix} \tag{3.13}$$

from where the D_s-optimality criterion to be minimized is

$$\Psi(\mathbf{M}) = \ln\det(\mathbf{\Gamma}^{-1}) = \ln\det((\mathbf{M}_{11} - \mathbf{M}_{12}\mathbf{M}_{22}^{-1}\mathbf{M}_{21})^{-1}) \tag{3.14}$$

which is equivalent to minimizing

$$\Psi(\mathbf{M}) = -\ln\det(\mathbf{M}_{11} - \mathbf{M}_{12}\mathbf{M}_{22}^{-1}\mathbf{M}_{21}). \tag{3.15}$$

3.3 Formulating an optimization problem

We seek to find the optimal sensor positions for our magnetic tracking system when the transmitter is within the measurement domain $\Omega_{\mathbf{p}}$, which is a limited part of the complete parameter space. Thus, we wish to solve

$$\begin{aligned} \underset{\vec{r}_k}{\text{minimize}} \quad & \Psi(\mathbf{M}(\mathbf{p}; \vec{r}_1, \ldots, \vec{r}_{N^{\text{rec}}})) = -\ln\det(\mathbf{M}(\mathbf{p}; \vec{r}_1, \ldots, \vec{r}_{N^{\text{rec}}})) \\ \text{subject to} \quad & \mathbf{p} \in \Omega_{\mathbf{p}} \\ & k = 1, \ldots, N^{\text{rec}}. \end{aligned} \tag{3.16}$$

Three major problems are common when solving problems of this type [18]:

1. **High dimensionality of the multimodal optimization problem**
   In the case of a planar sensor array, there are two coordinates to determine for each sensor wherefore the number of parameters to optimize is $2N^{\text{rec}}$. The cost function may also contain many local minima which makes it hard to find a global optimum.

2. **Sensor clusterization**
   As a consequence of the assumption of uncorrelated noise between measurements, sensors could end up close to or on top of each other in the optimal solution. This is not desired in general since the assumption of uncorrelated noise is not true for several sensor types when the sensors are close to each other (cf. mutual coupling in the magnetic tracking case). Furthermore, technical limitations may set limits to how closely spaced the sensors can be.

3. **Dependence of the solution on the parameters to be identified**
   In the formulation of $\mathbf{M}$, we linearize the expression for the measured voltages around a certain point in the measurement domain. However, the linearization is only valid in a small region around this point, a region that usually is smaller than the measurement domain.

In this work, we restrain ourselves to a measurement domain which only includes one point. This point can then be moved to different positions in the measurement domain of the system we want to model. Inclusion of the entire measurement domain will be carried out in our future work, see section 5.

3.4 Sensor selection

One way to alleviate the sensor clusterization problem, when solving the optimization problem (3.16), is to specify a finite number J of allowed sensor positions. The problem is thereby changed into a combinatorial one

$$\begin{aligned} \underset{w_j}{\text{minimize}} \quad & -\ln\det\left(\sum_{j=1}^{J} w_j \mathbf{M}_j(\mathbf{p})\right) \\ \text{subject to} \quad & \mathbf{p} \in \Omega_{\mathbf{p}} \\ & w_j \in \{0,1\}, \quad j = 1,\ldots,J \\ & \sum_j w_j = N^{\text{rec}} \end{aligned} \tag{3.17}$$

where we seek which N^{rec} sensors among the J candidates to use ($w_j = 1$). There are $\binom{J}{N^{\text{rec}}}$ combinations wherefore an exhaustive search is tractable only for small problems.

An approximate solution to the problem in equation (3.17) can be obtained by relaxing the constraint on the weights [34] so that they become real numbers instead

of integers, that is

$$\begin{aligned} \underset{w_j}{\text{minimize}} \quad & -\ln\det\left(\sum_{j=1}^{J} w_j \mathbf{M}_j(\mathbf{p})\right) \\ \text{subject to} \quad & \mathbf{p} \in \Omega_{\mathbf{p}} \\ & w_j \in [0,1], \quad j = 1,\ldots,J \\ & \sum_j w_j = N^{\text{rec}}. \end{aligned} \tag{3.18}$$

The relaxed problem is convex [34] and the possible multimodality of the optimization problem has thereby been removed. The value of the cost function of the solution to the relaxed problem is clearly a lower bound to the same quantity of the non-relaxed problem since the feasible set of the non-relaxed problem is a subset of the relaxed problem's feasible set [35].

3.5 Number of sensors

In order to estimate p parameters, at least p independent measurements are needed. In our case $p = 5$ and, consequently, we need at least five sensors. However, sensors can be "blind" in some parts of the parameter space. For example, consider a transmitter oriented along the x-axis at $(0, 0, 1)$ and a line of sensors oriented along the z-axis positioned at $(x_i, 0, 0)$. Let the transmitter move an infinitesimal distance in the y-direction. The sensors will be unable to distinguish if the transmitter has moved in the positive or negative y-direction since the measured field stays constant, that is $\frac{\partial V_i}{\partial y^{\text{trans}}} = 0$. Similar problems are discussed by McGary et al. [36] for a system with two tri-axial sensors.

The parameter estimation can be successful even if some sensors are blind. However, unambiguous parameter estimation is not possible if the sensitivity matrix $\mathbf{G}$, defined in equation (3.4), does not have full rank. Thus, several vectors in the parameter space correspond to the same measured signals for a rank-deficient sensitivity matrix.

The minimum number of sensors needed is therefore p plus the maximum number of concurrently blinded sensors. Shafrir et al. [16] employed differential evolution (a type of evolutionary algorithm) in a simulation-based maximization of the condition number of the sensitivity matrix and showed that unambiguous parameter estimation is not possible with five, six, or seven sensors for a magnetic tracking system with a flat sensor array. Plotkin et al. [12] claimed that not more than two sensors can be blinded simultaneously for their specific sensor layout which comprises eight sensors.

An interesting result on the number of sensors is obtained if the problem in equation (3.17) is modified slightly before being relaxed. Allow multiple measurements to be performed with the same sensor and let w_j denote the number of measurements

performed with sensor j. The number N^{rec} is now the total number of experiments. Introduce $\lambda_j = w_j/N^{\text{rec}}$ which is the fraction of the total number of measurement which is performed with sensor j. After relaxation (which can be easily motivated if the number of measurements is large), the problem is changed into

$$\begin{aligned} \underset{\lambda_j}{\text{minimize}} \quad & -\ln\det\left(\sum_{j=1}^{J}\lambda_j \mathbf{M}_j(\mathbf{p})\right) \\ \text{subject to} \quad & \mathbf{p}\in\Omega_{\mathbf{p}} \\ & \lambda_j > 0, \quad j=1,\ldots,J \\ & \sum_j \lambda_j = 1. \end{aligned} \tag{3.19}$$

By application of Caratheodory's theorem one can show, see reference [21], that the D-optimal solution uses at most $p(p+1)/2$ sensors. In general, for any choice of optimality criterion $\Psi(\mathbf{M})$, the maximum number of sensors is $[p(p+1)/2]+1$.

4 Results

4.1 Optimization of a circular sensor array

4.1.1 D-optimal sensor positions

We start by reducing the dimensionality of the optimization problem in (3.16) and confine our sensors to a circle of radius r on which the sensors are uniformly positioned. Furthermore, we reduce the measurement domain to a point, that is $\Omega_{\mathbf{p}} = \{\mathbf{p}_0\}$. The optimization problem we solve is thus

$$\begin{aligned} \underset{r}{\text{minimize}} \quad & \Psi(\mathbf{M}(\mathbf{p}; r)) = -\ln\det(\mathbf{M}(\mathbf{p}; r)) \\ \text{subject to} \quad & \mathbf{p} = \mathbf{p}_0. \end{aligned} \tag{4.1}$$

We solve the problem by performing an exhaustive search with a resolution in r of $0.01\, z_0$ where z_0 is the height of the implant above the sensor plane as shown in figure 4.1. We compare the performance of sensor arrays with 5, 8, and 16 sensors. These numbers are used since 5 is the smallest number of sensors needed to estimate the five parameters in $\mathbf{p}$, 8 is the smallest number of sensors needed to avoid a degenerated problem according to Shafrir et al. [16], and 16 since it is the first even number larger than $p(p+1)/2 = 15$ which is the upper limit to the number of sensors used by a D-optimal solution to the problem in equation (3.19).

We solve the problem for two different transmitter positions. In the first, the transmitter is positioned straight above the center of the sensor circle, with a magnetic moment pointing along the y-axis, that is $\mathbf{p}_0 = [0, 0, z_0, 90°, 90°]^T$. In the second, the transmitter has been moved away from the circle center and it is making an angle to the sensor plane: $\mathbf{p}_0 = [z_0/3, z_0/3, z_0, 70°, 90°]^T$. The non-centered (second) transmitter position is shown in figure 4.1.

The cost function is given in figure 4.2 for the centered transmitter position as a function of the normalized radius of the array, r/z_0. The left hand plot of figure 4.2 shows that optimal performance is given by an array which is neither too small nor too large. This result agrees well with the intuitive idea that the sensors of a small array will collect similar information whereas a large array will suffer from low signal levels due to the increased distance between the transmitter and the sensors. An optimal array size will have the best balance between these two effects. In our case, this balance is achieved for a radius of $0.47\, z_0$ for all three arrays. Clearly, an array with a large number of sensors will perform better than an array with fewer sensors due to the impact from noise being reduced by averaging. We have therefore normalized the cost function with respect to the number of sensors in the right hand plot of figure 4.2 by using the identity

$$\det(x\mathbf{A}) = x^p \det \mathbf{A} \tag{4.2}$$

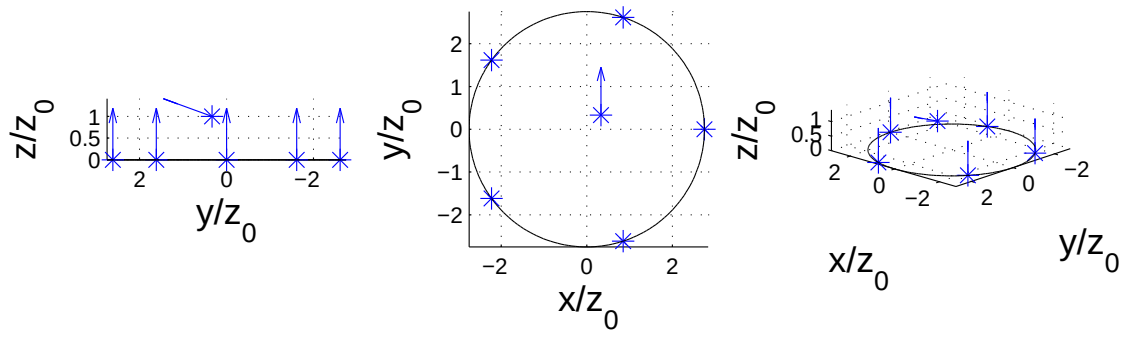

Figure 4.1. Circular sensor array with five sensors and a non-centered transmitter. Sensor and transmitter positions are indicated by stars whereas arrows show the orientation of their magnetic moments.

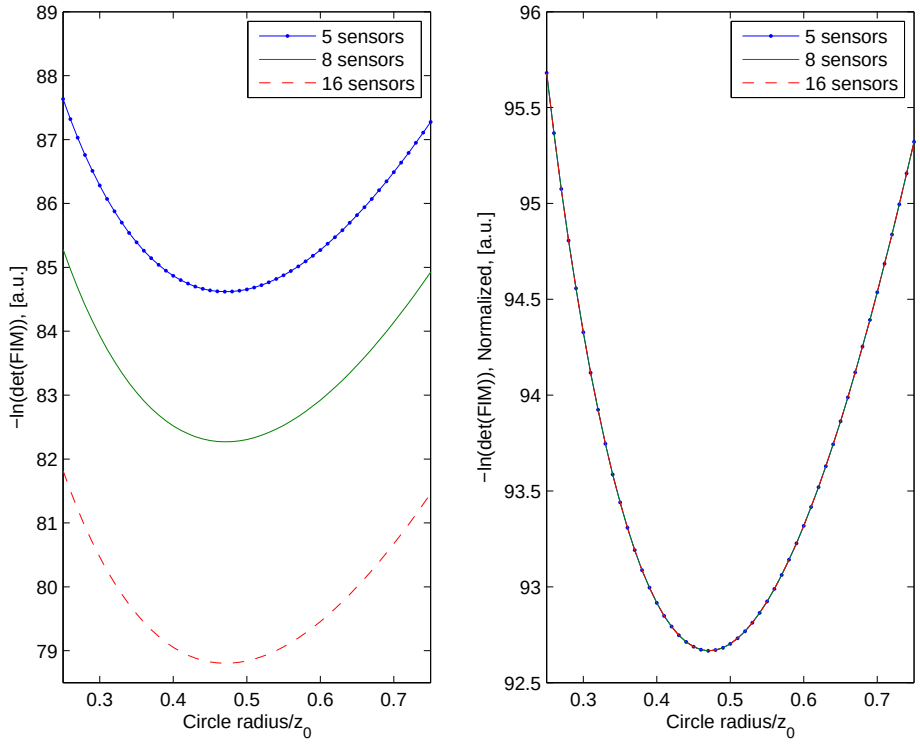

Figure 4.2. Cost function for a circular sensor array with 5, 8, and 16 sensors as a function of array radius, without (*left*) and with (*right*) normalization with respect to the number of sensors for a centered transmitter. The radius has been normalized with respect to the transmitter height above the sensor plane (z_0).

where $\mathbf{A}$ is $p \times p$. The normalized cost function is thus

$$-\ln\det(\mathbf{M}(\mathbf{p})) + p\ln(N^{\text{rec}}) = -\ln\det\left(\frac{\mathbf{M}(\mathbf{p})}{N^{\text{rec}}}\right) \tag{4.3}$$

where N^{rec} is the number of sensors. The normalized cost function does not change if a sensor is added to the array in the same place as an already existing sensor. As

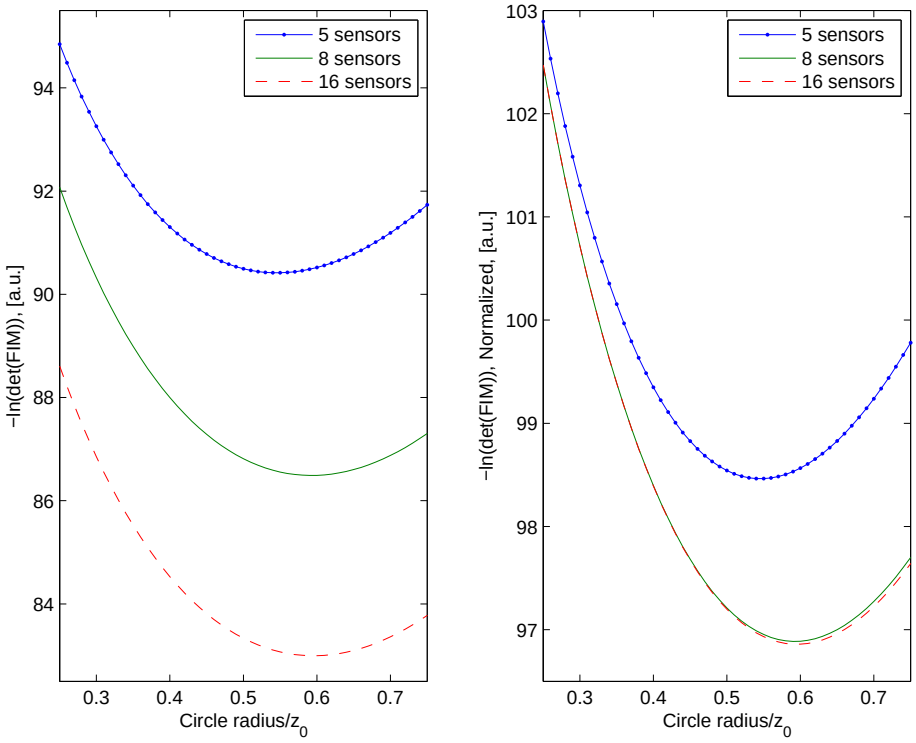

Figure 4.3. Cost function for a circular sensor array with 5, 8, and 16 sensors as a function of array radius, without (*left*) and with (*right*) normalization with respect to the number of sensors for a non-centered transmitter. The radius has been normalized with respect to the transmitter height above the sensor plane (z_0).

can be seen in the figure, additional sensors added after the first five only provide an improvement in the averaging of noise and does not provide any new information.

The cost function for the non-centered implant is shown in figure 4.3. The optimal radius is $[0.55, 0.59, 0.60] * z_0$ for an array with 5, 8, and 16 sensors respectively. Furthermore, the right hand plot in the figure shows that new information is gained by an increase in the number of sensors from 5 to 8. A similar, but much smaller gain, is obtained by an increase from 8 to 16 sensors.

The cost function behaves similarly if an infinite PMC plane is added $0.085\, z_0$ below the plane with the sensors. The optimal value of the radius is now $0.5\, z_0$ for the centered case and $[0.57, 0.62, 0.62] * z_0$ for the non-centered case. In addition, the minimum value of the cost function is lower with the PMC plane than without it. An explanation could be that the PMC plane increases the measured signal strength and, therefore, the sensors can move further away from the transmitter to receive more diverse information.

	Free space			PMC plane		
N^{rec}	D	D_s-position	D_s-angle	D	D_s-position	D_s-angle
5	$0.47z_0$	$0.55z_0$	$0.56z_0$	$0.50z_0$	$0.58z_0$	$0.60z_0$
8	$0.47z_0$	$0.55z_0$	$0.56z_0$	$0.50z_0$	$0.58z_0$	$0.60z_0$
16	$0.47z_0$	$0.55z_0$	$0.56z_0$	$0.50z_0$	$0.58z_0$	$0.60z_0$

Table 4.1. Optimal radius for a circular sensor array as a function of the number of sensors, optimality criterion, and presence of an infinite PMC plane. The transmitter is in the centered position.

	Free space			PMC plane		
N^{rec}	D	D_s-position	D_s-angle	D	D_s-position	D_s-angle
5	$0.55z_0$	$0.56z_0$	$0.75z_0$	$0.57z_0$	$0.59z_0$	$0.79z_0$
8	$0.59z_0$	$0.62z_0$	$0.73z_0$	$0.62z_0$	$0.65z_0$	$0.77z_0$
16	$0.60z_0$	$0.62z_0$	$0.73z_0$	$0.62z_0$	$0.65z_0$	$0.77z_0$

Table 4.2. Optimal radius for a circular sensor array as a function of the number of sensors, optimality criterion, and presence of an infinite PMC plane. The transmitter is in the non-centered position.

4.1.2 D_S-optimal sensor positions

We consider the same circular array and transmitter positions as in section 4.1.1 above and try to find the array radius that minimizes the D_s-criterion as described in equation (3.15). First, we optimize for the subset of $\mathbf{p}$ that contains the three spatial coordinates and refer to this as "D_s-position". Next, we perform a similar task for the two angular components and refer to this as "D_s-angle".

The cost function has similar shape for the D_s-optimality criteria as for the D-optimality criteria as shown in figures 4.2 and 4.3 above. The optimal radii are summarized in table 4.1 for the centered transmitter and in table 4.2 for the non-centered transmitter. Both choices of parameter subset for the D_s-criterion yield radii that are larger than the D-optimal radius. Of the D_s-optimal radii, the D_s-angle radius is consistently larger than the D_s-position. This result is in agreement with the results on page 47 in reference [16] where the sensor array optimized for orientation resolution is larger than the sensor array optimized for location resolution. As before, the optimal radius is larger for a non-centered transmitter than for a centered transmitter.

The addition of a PMC plane beneath the sensors causes the optimal radii to increase slightly regardless of which optimality criterion is used. The optimal radii are presented in table 4.1 for the centered transmitter position and in table 4.2 for the non-centered transmitter position.

It is interesting to note that the D-optimal radius is not a convex combination of the D_s-position radius and the D_s-angle radius, instead it is smaller than both of

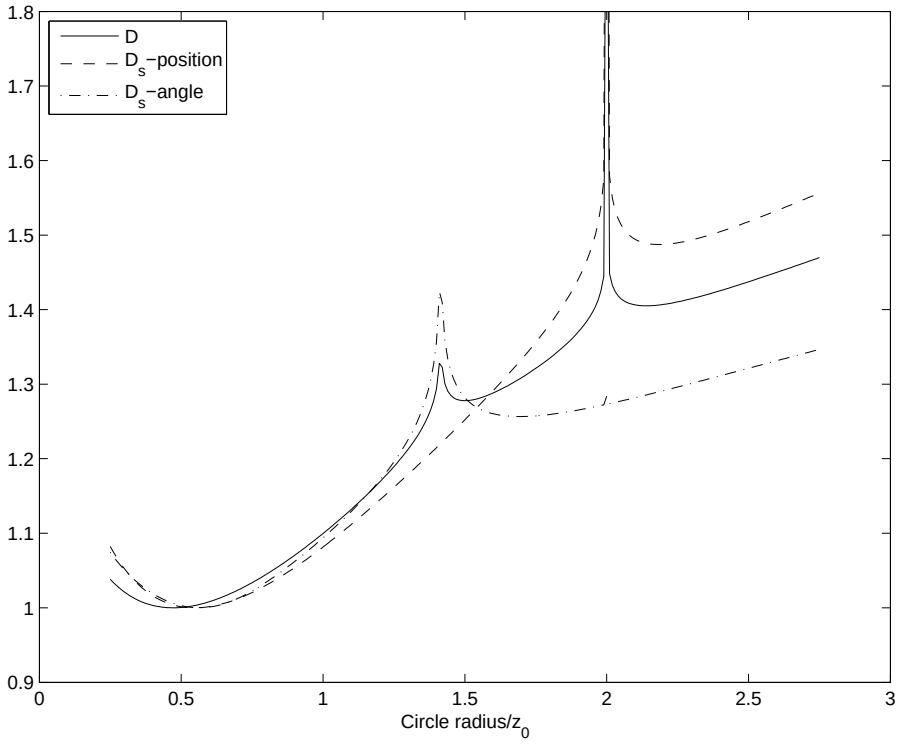

Figure 4.4. Cost functions for different optimality criteria and a circular sensor array with 16 sensors as a function of array radius. The cost functions have been normalized by division with their minimum value. The radius has been normalized with respect to the transmitter height above the sensor plane (z_0). The transmitter is in the centered position and there is no PMC plane.

them.

Figure 4.4 shows the cost functions for the D, D_s-position, and D_s-angle optimality criteria for a centered transmitter where the radius of the array has been varied over a larger interval than before. The peaks in the curves show when the problem degenerates. For example, for a radius of 1.41 z_0, the transmitter orientation is nearly impossible to determine as showed by the peak in the D_s-angle curve. Similarly, the transmitter position is difficult to estimate for a radius of 2.00 z_0, as shown by the peak in the D_s-position curve. Peaks are present at both these radii for the curve associated with the D-optimality criterion.

4.2 Optimization of a planar sensor array

Consider a planar sensor array consisting of 2009 sensors placed on a Cartesian grid with $|x| \leq 100\,\text{mm}$, $|y| \leq 120\,\text{mm}$ and a cell size of 5 mm in each direction.

Furthermore, consider a measurement domain $\Omega_{\mathbf{p}}$ defined by

$$\begin{aligned} x &\in [-50, 50]\,\text{mm}, \\ y &\in [-50, 50]\,\text{mm}, \\ z &\in [100, 200]\,\text{mm}, \\ \theta &\in [70^\circ, 110^\circ], \\ \varphi &\in [70^\circ, 110^\circ]. \end{aligned} \tag{4.4}$$

We wish to solve the sensor selection problem in equation (3.18) for this sensor array and measurement domain. The problem is simplified by reducing the measurement domain to a point. However, we will investigate how the solution changes for different positions of the point in the measurement domain. To solve the sensor selection problem in equation (3.18), we use `CVX`, a package for specifying and solving convex programs [37, 38].

By symmetry, a translation of the transmitter parallel to the sensor plane and a rotation of the transmitter around the z-axis result in a similar transformation of the sensor weights as long as the sensor candidates' positions permit such a transformation. Thus, the impact of x, y, and φ on the sensor weights is understood and, therefore, we investigate the impact of z and θ in the following.

The sensor selection problem is solved for the two extreme values of z in $\Omega_{\mathbf{p}}$. For a transmitter located close to the sensor plane with $\mathbf{p} = [0\,\text{cm}, 0\,\text{cm}, 10\,\text{cm}, 90^\circ, 90^\circ]^T$, the optimal distribution of weights is shown in the left-hand part of figure 4.5. The right-hand part of the same figure shows the positions of the 8 sensors with largest weights. These weights constitute 68.6 % of the total sum of weights.

Similarly, for a transmitter positioned far away from the sensor plane with $\mathbf{p} = [0\,\text{cm}, 0\,\text{cm}, 20\,\text{cm}, 90^\circ, 90^\circ]^T$, the optimal distribution of weights and the positions of the 8 sensors with largest weights are shown in figure 4.6. In this case, the 8 largest weights constitute 84.2 % of the total sum of weights. In figures 4.5 and 4.6 we see that the distribution of weights consists of a few peaks surrounded by values which are close to zero. There are 6 peaks in both figures wherefore the optimal number of sensors for this transmitter position is 6 if the noise averaging effect is neglected. This is also reflected by the positions of the sensors with largest weights, where we see that the sensors cluster around the 6 best positions.

Some of the best sensor positions seem to be located on straight lines parallel with the x- and y-axes. This might not be the case if the cell size of the sensor grid is decreased.

The distance between the transmitter and the sensor plane is double for the results in figure 4.6 as compared to the situation for the results in figure 4.5. Similarly, the distance from the origin to the optimal sensor positions have doubled and the sensor pattern in figure 4.6 is just a radially scaled version of the pattern in figure 4.5 when clusterization effects and cell size have been compensated for.

The impact of the transmitter orientation is illustrated by the result for a transmitter

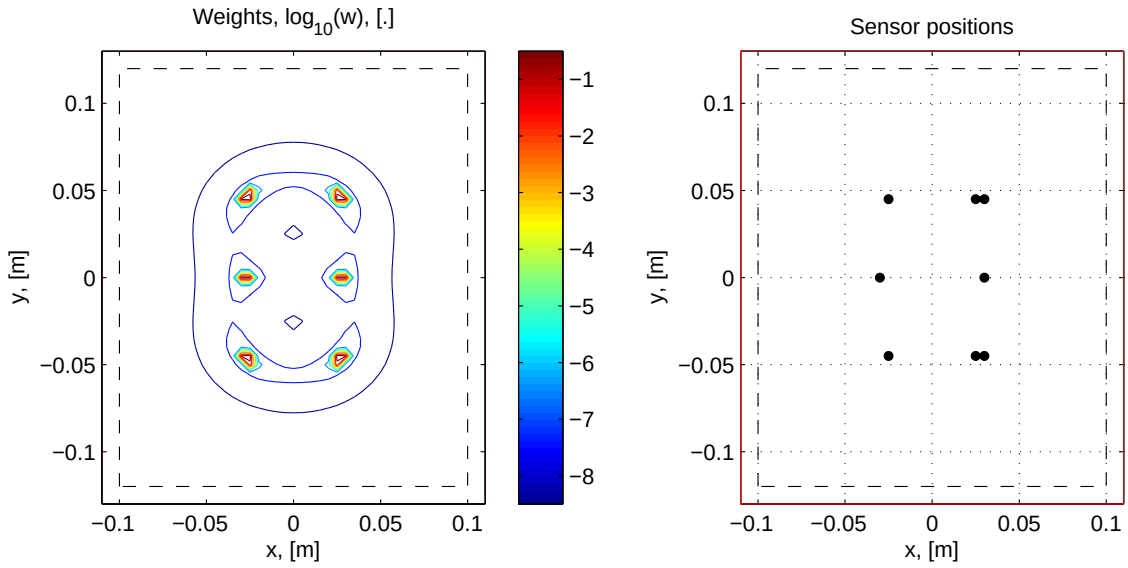

Figure 4.5. Optimal sensor weights (*left*) and sensor positions of the 8 sensors with largest weights (*right*) for a transmitter situated at $\mathbf{p} = [0\,\text{cm}, 0\,\text{cm}, 10\,\text{cm}, 90°, 90°]^T$.

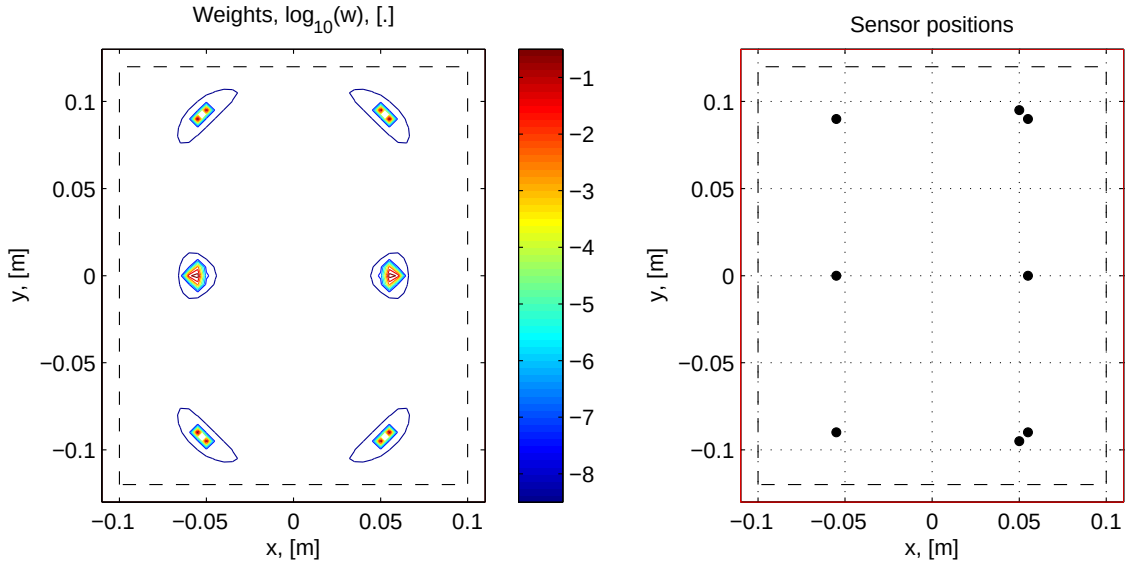

Figure 4.6. Optimal sensor weights (*left*) and sensor positions of the 8 sensors with largest weights (*right*) for a transmitter situated at $\mathbf{p} = [0\,\text{cm}, 0\,\text{cm}, 20\,\text{cm}, 90°, 90°]^T$.

situated at $\mathbf{p} = [0\,\text{cm}, 0\,\text{cm}, 20\,\text{cm}, 70°, 90°]^T$ as shown in figure 4.7. The rectangular shape of the sensor positions obtained for $\theta = 90°$ has now turned into a conical one. The sensors positioned in the half-plane at which the transmitter is pointing downwards have approached the midline $x = 0$ whereas the sensors in the opposite half-plane have moved away from the midline. It is also interesting to note that the

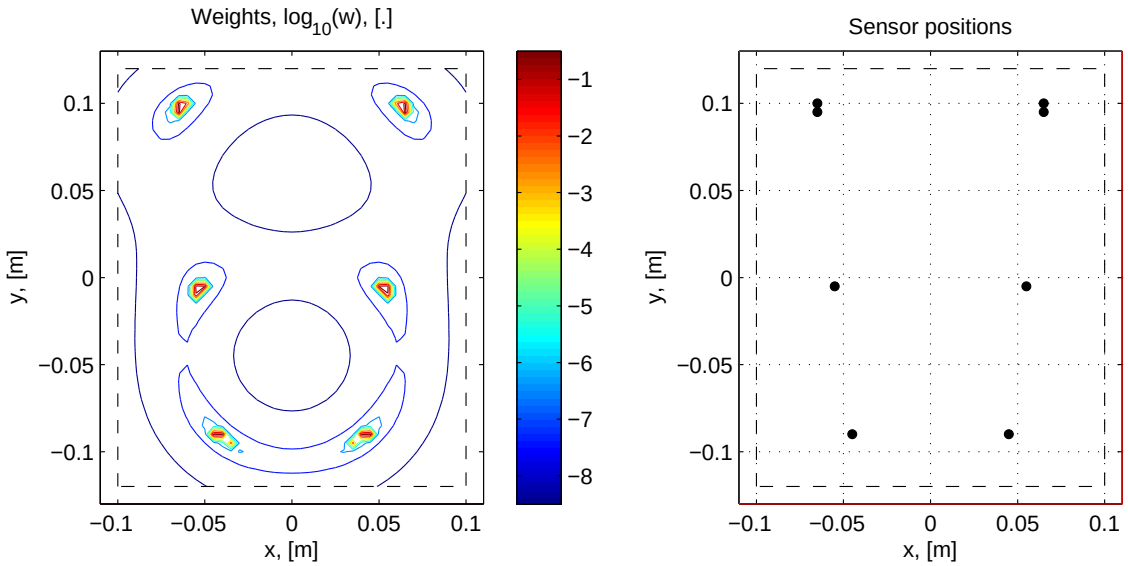

Figure 4.7. Optimal sensor weights (*left*) and sensor positions of the 8 sensors with largest weights (*right*) for a transmitter situated at $\mathbf{p} = [0\,\text{cm}, 0\,\text{cm}, 20\,\text{cm}, 70°, 90°]^T$.

sensors formerly on the line $y = 0$ have moved into the lower half-plane. For this transmitter position 70.5 % of the total weight is used by the 8 sensors with largest weights.

In conclusion, the positions and pattern of the sensor array with optimally placed sensors depends on the position and orientation of the transmitter. For a transmitter oriented in parallel with the sensor plane, the optimal sensor configuration is a rectangle with sensors at the corners and at the midpoints of the long sides. A movement of the transmitter in the x- and y-directions corresponds to a similar movement of the sensors. If the transmitter is rotated around the z-axis, i.e. φ is changed, so are the optimal sensor positions. An increase in the transmitters z-coordinate causes the sensor positions to move away from the origin. Finally, rotating the transmitter by changing θ causes the sensor rectangle to assume the shape of a part of a cone.

Clearly, it is not a trivial task to optimize the sensor positions for an arbitrary measurement domain, which is discussed further in section 5.

5 Conclusion

In this work, the sensor positions of a magnetic tracking system were optimized by exploiting a model where the transmitting and receiving coils of the system were approximated by magnetic dipoles. The model can also include an infinite PMC plane that is modeled with the method of images.

In order to compare different sensor array layouts, performance measures based on the Fisher information matrix (FIM) were discussed. Two optimality criteria acting on the FIM were exploited, namely D- and the D_s-optimality, and compared for the optimization of the sensor positions of a circular sensor array. Furthermore, a normalized version of the D-optimality criterion was proposed to measure the additional information added by a sensor apart from its contribution to the averaging of noise.

The sensor position problem was formulated as an optimization problem which was cast as a sensor selection problem. The sensor selection problem was solved by the application of a convex relaxation. The convex optimization problem was solved for a planar sensor array. Several transmitter positions were considered and general results were established for the dependence of the optimal sensor positions on the transmitter's position and orientation.

Our future work includes the following items:

- Further investigation on performance measures.
- Optimization for a complete measurement domain, also known as robust designs. This is based on a design decision: should the average accuracy, the accuracy in the worst case (so-called minimax designs), or some other quantity be considered? Several techniques exist in the literature for solving these types of problems as described in references [16, 18, 21, 35].
- Local optimization can in some cases improve the approximate solution obtained from the relaxed problem. See, for example, the sensor exchanging scheme in reference [35].

Bibliography

[1] R. Iustin, J. Linder, E. Isberg, T. Gustafsson, and B. Lennernäs. A Model Based Positioning System. Patent. WO 2008/079071 A1, World Intellectual Property Organization, 2008.

[2] A Plotkin, O Shafrir, E Paperno, and D.M. Kaplan. Magnetic eye tracking: A new approach employing a planar transmitter. *IEEE transactions on biomedical engineering*, 57(5):1209–1215, March 2010.

[3] Jeremy A. Baldoni and Benjamin B. Yellen. Magnetic Tracking System: Monitoring Heart Valve Prostheses. *IEEE Transactions on Magnetics*, 43(6):2430–2432, June 2007.

[4] J M Gilbert, S I Rybchenko, R Hofe, S R Ell, M J Fagan, R K Moore, and P Green. Isolated word recognition of silent speech using magnetic implants and sensors. *Medical engineering & physics*, 32(10):1189–97, December 2010.

[5] Wan'an Yang, Chao Hu, Max Q.-H. Meng, Shuang Song, and Houde Dai. A Six-Dimensional Magnetic Localization Algorithm for a Rectangular Magnet Objective Based on a Particle Swarm Optimizer. *IEEE Transactions on Magnetics*, 45(8):3092–3099, August 2009.

[6] Sascha Krueger, Holger Timinger, Ruediger Grewer, and Joern Borgert. Modality-integrated magnetic catheter tracking for x-ray vascular interventions. *Physics in Medicine and Biology*, 50(4):581–597, February 2005.

[7] Biosense Webster. Carto 3 System. `www.biosensewebster.com/products/navigation/carto3.aspx`, Accessed Oct. 17, 2011.

[8] Jason T. Sherman, Jonathan K. Lubkert, Radivoje S. Popovic, and Mark R. DiSilvestro. Characterization of a Novel Magnetic Tracking System. *IEEE Transactions on Magnetics*, 43(6):2725–2727, June 2007.

[9] Yue Liu, Yongtian Wang, Dayuan Yan, and Ya Zhou. DPSD algorithm for AC magnetic tracking system. In *2004 IEEE Symposium on Virtual Environments, Human-Computer Interfaces and Measurement Systems, 2004. (VCIMS).*, pages 101–106. IEEE, 2004.

[10] Frederick Raab, Ernest Blood, Terry Steiner, and Herbert Jones. Magnetic Position and Orientation Tracking System. *IEEE Transactions on Aerospace and Electronic Systems*, AES-15(5):709–718, September 1979.

[11] Darmindra D Arumugam, Joshua D Griffin, and Daniel D Stancil. Experimental Demonstration of Complex Image Theory and Application to Position Measurement. *IEEE Antennas and Wireless Propagation Letters*, 10:282–285, 2011.

[12] A. Plotkin and E. Paperno. 3-D magnetic tracking of a single subminiature coil with a large 2-D array of uniaxial transmitters. *IEEE Transactions on Magnetics*, 39(5):3295–3297, September 2003.

[13] E. Paperno and P. Keisar. Three-Dimensional Magnetic Tracking of Biaxial Sensors. *IEEE Transactions on Magnetics*, 40(3):1530–1536, May 2004.

[14] Anton Plotkin, Eugene Paperno, and Netzer Moriya. Relationship between the Measurement and Motion Bandwidths in Magnetic Tracking. *2006 IEEE Instrumentation and Measurement Technology Conference Proceedings*, pages 2165–2170, April 2006.

[15] T. Nara, S. Suzuki, and S. Ando. A Closed-Form Formula for Magnetic Dipole Localization by Measurement of Its Magnetic Field and Spatial Gradients. *IEEE Transactions on Magnetics*, 42(10):3291–3293, October 2006.

[16] Oren Shafrir, Eugene Paperno, and Anton Plotkin. *Magnetic Tracking with a Flat Transmitter*. Lambert Academic Publishing, 2010.

[17] V Schlageter, P.-A. Besse, R.S. Popovic, and P. Kucera. Tracking system with five degrees of freedom using a 2D-array of Hall sensors and a permanent magnet. *Sensors and Actuators A: Physical*, 92(1-3):37–42, August 2001.

[18] D Ucinski. *Optimal measurement methods for distributed parameter system identification*. CRC Press LLC, Boca Raton, 2005.

[19] F Pukelsheim. *Optimal design of experiments*. Classics in applied mathematics. SIAM/Society for Industrial and Applied Mathematics, 2006.

[20] A.C. Atkinson, A.N. Donev, and R. Tobias. *Optimum experimental designs, with SAS*, volume 34. Oxford University Press, USA, 2007.

[21] É Walter and L Pronzato. *Identification of parametric models from experimental data*. Communications and control engineering. Springer, 1997.

[22] J.S. Abel. Optimal sensor placement for passive source localization. *International Conference on Acoustics, Speech, and Signal Processing*, pages 2927–2930, 1990.

[23] H Zhang. Two-dimensional optimal sensor placement. *IEEE Transactions on Systems, Man, and Cybernetics*, 25(5):781–792, May 1995.

[24] S Martinez and F Bullo. Optimal sensor placement and motion coordination for target tracking. *Automatica*, 42(4):661–668, April 2006.

[25] Sven Nordebo and Mats Gustafsson. On the Design of Optimal Measurements for Antenna Near-Field Imaging Problems. In *AIP Conference Proceedings*, volume 834, pages 234–249. AIP, 2006.

[26] D. Roetenberg, P. Slycke, A. Ventevogel, and P.H. Veltink. A portable magnetic position and orientation tracker. *Sensors and Actuators A: Physical*, 135(2):426–432, April 2007.

[27] M Baszynski, Z Moron, and N Tewel. Electromagnetic navigation in medicine - basic issues, advantages and shortcomings, prospects of improvement. *Journal of Physics: Conference Series*, 238:012056, July 2010.

[28] Xin Ge, Dakun Lai, Xiaomei Wu, and Zuxiang Fang. A novel non-model-based 6-DOF electromagnetic tracking method using non-iterative algorithm. *International Conference of the IEEE Engineering in Medicine and Biology Society*, 2009:5114–7, January 2009.

[29] Anton Plotkin, Vladimir Kucher, Yoram Horen, and Eugene Paperno. A New Calibration Procedure for Magnetic Tracking Systems. *IEEE Transactions on Magnetics*, 44(11):4525–4528, November 2008.

[30] Mao Li, Shuang Song, Chao Hu, Wanan Yang, Lujia Wang, and Max Q.-H. Meng. A new calibration method for magnetic sensor array for tracking capsule endoscope. In *2009 IEEE International Conference on Robotics and Biomimetics (ROBIO)*, pages 1561–1566. IEEE, December 2009.

[31] E Paperno and A Plotkin. Cylindrical induction coil to accurately imitate the ideal magnetic dipole. *Sensors and Actuators A: Physical*, 112(2-3):248–252, May 2004.

[32] David K. Cheng. *Fundamentals of Engineering Electromagnetics*. Addison-Wesley Publishing Company, 1st edition, 1993.

[33] J.T. Weaver. Image theory for an arbitrary quasi-static field in the presence of a conducting half space. *Radio Science*, 6(6):647–653, 1971.

[34] Stephen Boyd and Lieven Vandenberghe. *Convex optimization*. Cambridge University Press, UK, 2004.

[35] Siddharth Joshi and Stephen Boyd. Sensor Selection via Convex Optimization. *IEEE Transactions on Signal Processing*, 57(2):451–462, February 2009.

[36] John E. McGary. Real-Time Tumor Tracking for Four-Dimensional Computed Tomography Using SQUID Magnetometers. *IEEE Transactions on Magnetics*, 45(9):3351–3361, September 2009.

[37] M Grant and S Boyd. CVX: Matlab Software for Disciplined Convex Programming, version 1.21. `http://cvxr.com/cvx`, April 2011.

[38] M Grant and S Boyd. Graph implementations for nonsmooth convex programs. In V Blondel, S Boyd, and H Kimura, editors, *Recent Advances in Learning and Control*, Lecture Notes in Control and Information Sciences, pages 95–110. Springer-Verlag Limited, 2008.